

# Statistical regimes of electromagnetic wave propagation in randomly time-varying media

Seulong Kim

*Research Institute of Basic Sciences, Ajou University, Suwon 16499, South Korea*

Kihong Kim\*

*Department of Physics, Ajou University, Suwon 16499, South Korea and  
School of Physics, Korea Institute for Advanced Study, Seoul 02455, South Korea*

(Dated: July 16, 2025)

Wave propagation in time-varying media enables unique control of energy transport by breaking energy conservation through temporal modulation. Among the resulting phenomena, temporal disorder—random fluctuations in material parameters—can suppress propagation and induce localization, analogous to Anderson localization. However, the statistical nature of this process remains incompletely understood. We present a comprehensive analytical and numerical study of electromagnetic waves in spatially uniform media with randomly time-varying permittivity. Using the invariant imbedding method, we derive exact moment equations and identify three distinct statistical regimes for initially unidirectional input: gamma-distributed energy at early times, exponential behavior at intermediate times, and a quasi-log-normal distribution at long times. In contrast, symmetric bidirectional input yields true log-normal statistics across all time scales. These findings are validated by extensive calculations using two complementary disorder models—delta-correlated Gaussian noise and piecewise-constant fluctuations—demonstrating that the observed statistics are robust and governed by input symmetry and temporal dynamics. Momentum conservation further constrains long-term behavior, linking initial conditions to energy growth. Our results establish a unified framework for understanding statistical wave dynamics in time-modulated systems and offer guiding principles for the design of dynamically tunable photonic and electromagnetic devices.

## I. INTRODUCTION

Wave propagation in time-varying media has emerged as a fertile ground for uncovering fundamentally new physical phenomena that are unattainable in static or spatially inhomogeneous systems [1–4]. In contrast to stationary media, where energy is conserved, time-dependent systems break energy conservation due to the explicit temporal variation of material parameters. This leads to unconventional scattering dynamics, temporal energy amplification, and novel mechanisms for controlling wave transport. Such effects are increasingly relevant in modern optics, materials science, and communication technologies, where temporal modulation enables dynamic functionalities beyond the capabilities of static systems.

Recent advances have revealed a variety of phenomena unique to time-varying systems, including temporal photonic crystals, momentum band gaps, temporal Brewster effects, temporal holography, and ultrafast wave steering [5–37]. Among these, temporal disorder—random fluctuations in material properties over time—has drawn particular attention for its striking analogy to Anderson localization in spatially disordered media [38–45]. Temporal disorder can induce strong localization effects, leading to the suppression of wave propagation. These effects are of both fundamental interest and practical importance,

with potential applications in ultrafast switching, energy harvesting, and temporally gated information processing.

Despite growing interest, the statistical behavior of waves in randomly time-varying media remains incompletely understood. Previous studies suggest that energy distributions may evolve from exponential forms at short times to log-normal distributions at longer times [39]. However, key questions remain unresolved: What governs the transition between these regimes? Is log-normal behavior truly universal? And how do initial wave conditions influence the statistical evolution?

In this work, we present a comprehensive analytical and numerical study of electromagnetic wave propagation in isotropic, spatially uniform media with randomly time-varying permittivity. Using the invariant imbedding method [45–47], we derive exact moment equations for reflectance, transmittance, and total energy density. For unidirectional input, our analysis reveals three distinct statistical regimes: gamma-distributed energy at early times, exponential behavior at intermediate times, and a quasi-log-normal distribution at long times—exhibiting systematic deviations from true log-normality. In contrast, symmetric bidirectional input produces log-normal statistics across all timescales.

These findings are supported by extensive numerical simulations based on two complementary disorder models: delta-correlated Gaussian noise and piecewise-constant stepwise fluctuations. Both models confirm that wave statistics are highly sensitive to the initial input symmetry and the duration of temporal disorder. Our results establish a unified framework for understanding sta-

---

\* khkim@ajou.ac.kr

tistical fluctuations and localization phenomena in time-varying systems and provide practical guidance for the design of dynamically tunable photonic and electromagnetic devices.

## II. THEORY

We investigate electromagnetic wave propagation in an isotropic, spatially uniform medium with time-dependent properties. The electric displacement field  $D$  satisfies the wave equation

$$\frac{d}{dt} \left( \mu \frac{dD}{dt} \right) + \frac{\omega_0^2}{\epsilon} D = 0, \quad \omega_0 = ck, \quad (1)$$

where  $\epsilon$  and  $\mu$  are the permittivity and permeability, respectively,  $c$  is the speed of light in vacuum, and  $k$  is the constant wavenumber. We consider wave propagation along the  $x$  axis.

In a time-independent medium, field components evolve as  $\exp[i(kx \mp \omega t)]$ . When the material parameters vary with time, scattering occurs at temporal interfaces, generating reflected and transmitted components. We consider a unit-amplitude plane wave initially propagating in the  $+x$  direction. If  $\epsilon$  and  $\mu$  vary only within the interval  $0 \leq t \leq T$ , the displacement field is given by

$$D(t) = \begin{cases} e^{-i\omega_1 t}, & t < 0 \\ s(T)e^{-i\omega_2(t-T)} + r(T)e^{i\omega_2(t-T)}, & t > T \end{cases}, \quad (2)$$

where  $\omega_1 = \omega_0/\sqrt{\epsilon_1\mu_1}$  and  $\omega_2 = \omega_0/\sqrt{\epsilon_2\mu_2}$ , with  $\epsilon_{1,2}$  and  $\mu_{1,2}$  denoting the permittivity and permeability before and after the modulation, respectively. All parameters are assumed to be positive. The coefficients  $s(T)$  and  $r(T)$  represent the temporal transmission and reflection amplitudes.

Using the invariant imbedding method [45–47], we derive exact differential equations for  $r$  and  $s$  with respect to the imbedding parameter  $\tau$ , which represents the duration of temporal variation:

$$\frac{1}{\omega_0} \frac{dr}{d\tau} = i\beta r + i\alpha s, \quad \frac{1}{\omega_0} \frac{ds}{d\tau} = -i\alpha r - i\beta s, \quad (3)$$

where

$$\alpha = \frac{1}{2n_2} \left( \frac{\epsilon_2}{\epsilon} - \frac{\mu_2}{\mu} \right), \quad \beta = \frac{1}{2n_2} \left( \frac{\epsilon_2}{\epsilon} + \frac{\mu_2}{\mu} \right), \quad (4)$$

and  $n_2 = \sqrt{\epsilon_2\mu_2}$ . The initial conditions at  $\tau = 0$ , corresponding to a sudden temporal interface, are given by

$$r(0) = \frac{1}{2} \left( 1 - \sqrt{\frac{\epsilon_2\mu_1}{\epsilon_1\mu_2}} \right), \quad s(0) = \frac{1}{2} \left( 1 + \sqrt{\frac{\epsilon_2\mu_1}{\epsilon_1\mu_2}} \right). \quad (5)$$

From Eq. (3), it follows that the difference between the squared magnitudes of the transmission and reflection amplitudes remains invariant during the temporal

modulation:

$$|s(\tau)|^2 - |r(\tau)|^2 = |s(0)|^2 - |r(0)|^2 = \sqrt{\frac{\epsilon_2\mu_1}{\epsilon_1\mu_2}}. \quad (6)$$

We define the temporal transmittance  $S$  and reflectance  $R$  as

$$S = \sqrt{\frac{\epsilon_1\mu_2}{\epsilon_2\mu_1}} |s|^2, \quad R = \sqrt{\frac{\epsilon_1\mu_2}{\epsilon_2\mu_1}} |r|^2. \quad (7)$$

It immediately follows that  $S - R = 1$  for arbitrary temporal variations of  $\epsilon$  and  $\mu$ . Since both  $S$  and  $R$  are nonnegative, we always have  $S \geq 1$ , indicating that total temporal reflection is not possible in isotropic media. In the special case of perfect transmission ( $R = 0$ ), we find  $S = 1$ , implying no amplification. It is important to note that  $S$  and  $R$  represent the ratios of photon number densities in the transmitted and reflected waves relative to the incident wave. This interpretation differs from the conventional definition based on energy flux.

In this study, we examine electromagnetic wave propagation in media where the dielectric permittivity  $\epsilon(t)$  varies randomly in time. Two stochastic models are considered. Model 1 assumes delta-correlated Gaussian noise:

$$\begin{aligned} \epsilon(t) &= \bar{\epsilon} + \delta\epsilon(t), \\ \langle \delta\epsilon(t)\delta\epsilon(t') \rangle &= g_0\delta(t-t'), \quad \langle \delta\epsilon(t) \rangle = 0, \end{aligned} \quad (8)$$

where  $\bar{\epsilon}$  is the mean permittivity and  $g_0$  (with units of time) quantifies the disorder strength. This model is analytically tractable and enables semi-analytical evaluation of all disorder-averaged moments. Model 2 describes piecewise-constant disorder: the fluctuation  $\delta\epsilon$  is constant within each time interval of duration  $\Lambda$ , and is abruptly updated at the end of each interval. Each new value is drawn independently from a uniform distribution over  $[-a_0, a_0]$ . The process continues over a total duration  $T$ . This model is particularly well suited for computing statistical quantities that are difficult to evaluate using Model 1, such as the moments of the logarithm of the wave energy and the full probability distributions of the logarithms of both the reflectance and the wave energy.

In Model 1, assuming weak disorder, we approximate the inverse permittivity as

$$\frac{1}{\epsilon} = \frac{1}{\bar{\epsilon} + \delta\epsilon} \approx \frac{1}{\bar{\epsilon}} - \frac{\delta\epsilon}{\bar{\epsilon}^2}. \quad (9)$$

Our goal is to compute the statistical moments of the transmittance, reflectance, and total wave energy density. To this end, we define the moment function  $Z_{abcd} = \langle r^a(r^*)^b s^c(s^*)^d \rangle$ , where  $a, b, c, d = 0, 1, 2, \dots$ . Applying Eq. (3) together with the Furutsu–Novikov formula [48, 49], we derive the following evolution equation for

$Z_{abcd}$ :

$$\begin{aligned} \frac{1}{\omega_0} \frac{d}{d\tau} Z_{abcd} = & C_1 Z_{abcd} + C_2 Z_{a+1,b,c-1,d} \\ & + C_3 Z_{a-1,b,c+1,d} + C_4 Z_{a,b+1,c,d-1} \\ & + C_5 Z_{a,b-1,c,d+1} + C_6 Z_{a+1,b+1,c-1,d-1} \\ & + C_7 Z_{a-1,b-1,c+1,d+1} + C_8 Z_{a+1,b-1,c-1,d+1} \\ & + C_9 Z_{a-1,b+1,c+1,d-1} + C_{10} Z_{a+2,b,c-2,d} \\ & + C_{11} Z_{a-2,b,c+2,d} + C_{12} Z_{a,b+2,c,d-2} \\ & + C_{13} Z_{a,b-2,c,d+2}, \end{aligned} \quad (10)$$

where the coefficients are given by

$$\begin{aligned} C_1 = & i\bar{\beta} (a - b - c + d) + \frac{g\gamma^2}{2} [a + b + c + d \\ & + 2ac + 2bd - (a - b - c + d)^2], \\ C_2 = & c [-i\bar{\alpha} + g\gamma^2 (a - b - c + d + 1)], \\ C_3 = & a [i\bar{\alpha} - g\gamma^2 (a - b - c + d - 1)], \\ C_4 = & d [i\bar{\alpha} - g\gamma^2 (a - b - c + d - 1)], \\ C_5 = & b [-i\bar{\alpha} + g\gamma^2 (a - b - c + d + 1)], \\ C_6 = & g\gamma^2 cd, \quad C_7 = g\gamma^2 ab, \\ C_8 = & -g\gamma^2 bc, \quad C_9 = -g\gamma^2 ad, \\ C_{10} = & -\frac{g\gamma^2}{2} c(c-1), \quad C_{11} = -\frac{g\gamma^2}{2} a(a-1), \\ C_{12} = & -\frac{g\gamma^2}{2} d(d-1), \quad C_{13} = -\frac{g\gamma^2}{2} b(b-1). \end{aligned} \quad (11)$$

The auxiliary parameters are defined as

$$\begin{aligned} \bar{\alpha} = & \frac{1}{2n_2} \left( \frac{\epsilon_2}{\bar{\epsilon}} - \frac{\mu_2}{\mu} \right), \quad \bar{\beta} = \frac{1}{2n_2} \left( \frac{\epsilon_2}{\bar{\epsilon}} + \frac{\mu_2}{\mu} \right), \\ \gamma = & \frac{1}{2n_2} \frac{\epsilon_2}{\bar{\epsilon}^2}, \quad g = g_0 \omega_0. \end{aligned} \quad (12)$$

The invariant imbedding method can be extended to more general cases in which plane waves with arbitrary relative amplitudes propagate simultaneously in opposite directions at the initial time. In this case, we generalize Eq. (2) and the initial conditions in Eq. (5) as follows:

$$\begin{aligned} D = & \begin{cases} s_i e^{-i\omega_1 t} + r_i e^{i\omega_1 t}, & \text{if } t < 0 \\ s(T) e^{-i\omega_2(t-T)} + r(T) e^{i\omega_2(t-T)}, & \text{if } t > T \end{cases}, \\ r(0) = & \frac{s_i}{2} \left( 1 - \sqrt{\frac{\epsilon_2 \mu_1}{\epsilon_1 \mu_2}} \right) + \frac{r_i}{2} \left( 1 + \sqrt{\frac{\epsilon_2 \mu_1}{\epsilon_1 \mu_2}} \right), \\ s(0) = & \frac{s_i}{2} \left( 1 + \sqrt{\frac{\epsilon_2 \mu_1}{\epsilon_1 \mu_2}} \right) + \frac{r_i}{2} \left( 1 - \sqrt{\frac{\epsilon_2 \mu_1}{\epsilon_1 \mu_2}} \right), \end{aligned} \quad (13)$$

where  $s_i$  and  $r_i$  denote the amplitudes of the incident waves propagating in the  $+x$  and  $-x$  directions, respectively, for  $t < 0$ . Under these generalized initial conditions, the invariant imbedding equations in Eqs. (3) and (10) remain valid and unchanged.

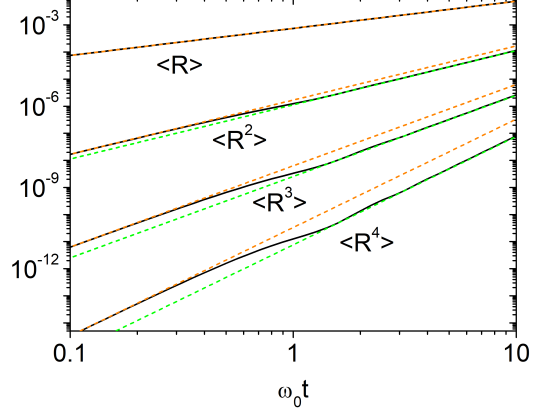


FIG. 1. Log-log plot of the temporal evolution of the reflectance moments  $\langle R \rangle$ ,  $\langle R^2 \rangle$ ,  $\langle R^3 \rangle$ , and  $\langle R^4 \rangle$  for Model 1 with  $g = 0.003$ . Numerical results from Eq. (10) are shown as black solid lines. The orange dashed lines represent the short-time behavior predicted by Eq. (14), while the green dashed lines correspond to the intermediate-time behavior described by Eq. (15). For  $n \geq 2$ , a clear crossover from the initial regime governed by Eq. (14) to the regime of Eq. (15) occurs near  $\omega_0 t \approx 1$ .

### III. RESULTS

We present the results of our numerical calculations. For simplicity, we focus on Model 1 with  $\epsilon_1 = \epsilon_2 = \bar{\epsilon} = 1$  and  $\mu_1 = \mu_2 = \mu = 1$ , under which the parameters in Eq. (12) simplify to  $\bar{\alpha} = 0$ ,  $\bar{\beta} = 1$ , and  $\gamma = 1/2$ . In this case, the reflectance and transmittance reduce to  $R = |r|^2$  and  $S = |s|^2$ , respectively.

The structure of Eq. (10) couples each moment  $Z_{abcd}$  to others with the same total indices, satisfying  $a' + c' = a + c$  and  $b' + d' = b + d$ . To compute  $Z_{nn00} = \langle R^n \rangle$  and  $Z_{00nn} = \langle S^n \rangle$ , it suffices to solve a finite system of  $(n+1)^2$  of coupled differential equations for the moments  $Z_{i,j,n-i,n-j}$ , where  $i, j = 0, 1, \dots, n$ .

When  $\epsilon_1 \mu_1 = \epsilon_2 \mu_2$ , the quantities  $R$  and  $S$  represent the reflected and transmitted energy densities, respectively, relative to the initial wave. The total energy density is then given by  $U = R + S = 2R + 1$ . The temporal evolution of the statistical moments depends on the time regime—short, intermediate, or long. For studying early-time dynamics, reflectance is a more sensitive observable than total energy, since  $R(0) = 0$  while  $U(0) = 1$ .

The evolution also depends on the initial wave conditions. In Fig. 1, we plot the first four moments of the reflectance in the short-time regime, assuming the wave initially propagates only in the forward direction [i.e.,  $r(0) = r_i = 0$ ,  $s(0) = s_i = 1$ ]. The corresponding initial condition is  $Z_{abcd}(0) = 1$  if  $a = b = 0$ , and zero otherwise.

Our numerical results show that, at early times, the

reflectance moments follow

$$\langle R^n \rangle = (2n-1)!! \left( \frac{g\omega_0 t}{4} \right)^n. \quad (14)$$

As time increases and  $\omega_0 t \approx 1$ , a crossover occurs to

$$\langle R^n \rangle = n! \left( \frac{g\omega_0 t}{4} \right)^n, \quad (15)$$

indicating a transition in the underlying probability distribution. At early times, the reflectance follows a gamma distribution:

$$P(R) = \frac{1}{\sqrt{\pi\theta R}} e^{-R/\theta}, \quad \theta = \frac{g\omega_0 t}{2}, \quad (16)$$

with moments

$$\langle R^n \rangle = \theta^n \frac{\Gamma(n + \frac{1}{2})}{\Gamma(\frac{1}{2})}. \quad (17)$$

As  $\omega_0 t$  increases to order unity, this distribution crosses over to an exponential form:

$$P(R) = \frac{2}{\theta} e^{-2R/\theta}, \quad (18)$$

with moments given by Eq. (15). This exponential regime persists up to  $\omega_0 t \lesssim g^{-1}$ .

Under the random phase approximation (RPA), which assumes

$$Z_{abcd} = 0, \text{ when } a \neq b \text{ and } c \neq d, \quad (19)$$

we find numerically that the reflectance moments exactly match those of the exponential distribution. This result, consistent with [39], confirms that under RPA, the reflectance indeed follows an exponential distribution.

In summary, in the intermediate regime  $1 \lesssim \omega_0 t \lesssim g^{-1}$ , the reflectance moments converge to those of an exponential distribution. This transition is driven by the randomization of the phases of  $r$  and  $s$ , which governs the underlying statistical behavior. The crossover from a gamma to an exponential distribution occurs near  $\omega_0 t \sim 1$  and is largely insensitive to disorder strength in the weak-disorder regime. The crossover time is inversely proportional to  $\omega_0 = ck$ .

We now examine the time evolution of the total wave energy, focusing primarily on the long-time regime. In Fig. 2, we present the first four moments of  $U$ , which show excellent agreement with the analytical expression

$$\langle U^n \rangle = \frac{n!}{(2n-1)!!} \exp \left[ n(n+1) \left( \frac{g\omega_0 t}{4} \right) \right], \quad (20)$$

valid over a broad temporal range,  $g^{-1} \lesssim \omega_0 t \lesssim 10^6$ . The case  $n = 1$  is exceptional. Numerical results confirm that the average wave energy is accurately described by

$$\langle U \rangle = \exp \left( \frac{g\omega_0 t}{2} \right), \quad (21)$$

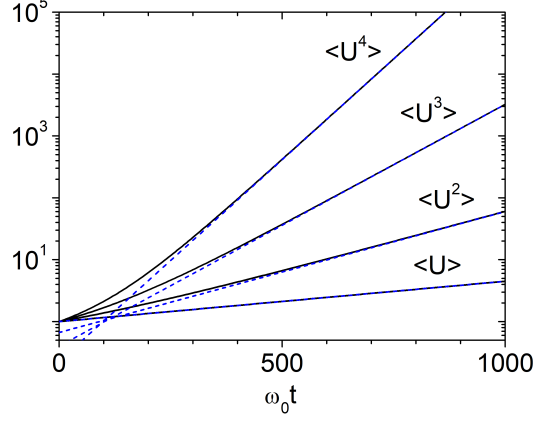


FIG. 2. Temporal growth of energy moments for  $g = 0.003$ . The evolution of  $\langle U \rangle$ ,  $\langle U^2 \rangle$ ,  $\langle U^3 \rangle$ , and  $\langle U^4 \rangle$  is shown. Solid lines represent numerical results from Eq. (10), and dashed lines show the analytical prediction from Eq. (20). Excellent agreement is observed in the long-time regime  $\omega_0 t \gtrsim g^{-1}$ .

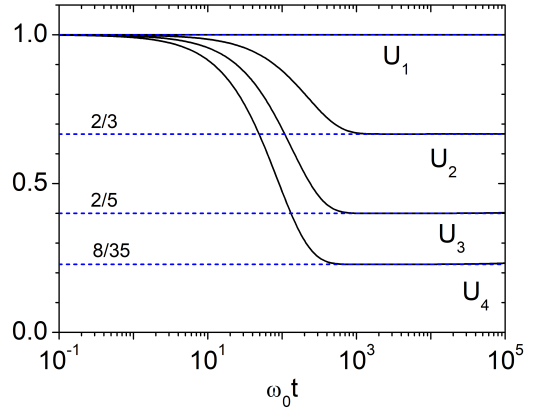


FIG. 3. Temporal variation of  $U_n$  for  $g = 0.003$ . Here,  $U_n = \langle U^n \rangle \exp[-n(n+1)g\omega_0 t/4]$ . In the long-time regime, numerical results show excellent agreement with the analytical predictions from Eq. (20).

throughout the entire interval  $0 < \omega_0 t \lesssim 10^6$ .

Although Eq. (20) resembles the raw moments of a log-normal distribution,

$$\langle U^n \rangle_{\text{LN}} = \exp \left[ n(n+1) \left( \frac{g\omega_0 t}{4} \right) \right], \quad (22)$$

the presence of the prefactor  $n!/(2n-1)!!$  in Eq. (20) distinguishes the actual distribution from a true log-normal form. While the two distributions become asymptotically similar as  $t \rightarrow \infty$ , significant deviations persist over a broad and experimentally relevant time range. This suggests that the underlying distribution is not strictly log-normal, but rather follows a form we refer to as a quasi-log-normal distribution.

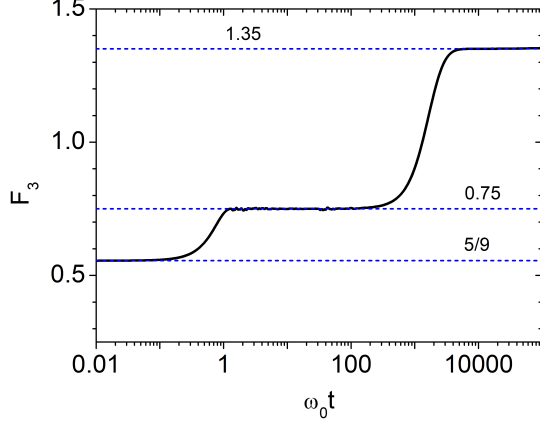


FIG. 4. Temporal evolution of  $F_3$  for  $g = 0.003$ .  $F_3 \equiv \langle R^3 \rangle \langle R \rangle^3 / \langle R^2 \rangle^3$  evolves from an initial value of  $5/9$  (gamma distribution), passes through  $0.75$  (exponential distribution), and approaches  $1.35$ , consistent with the quasi-log-normal form given in Eq. (20).

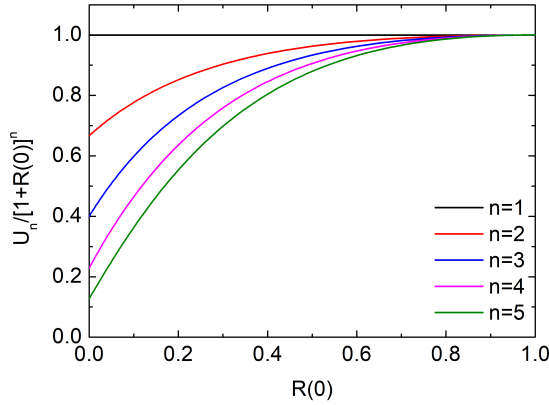


FIG. 5. Scaled moments  $U_n / [1 + R(0)]^n$  as functions of  $R(0) = |r_i|^2$  for  $n = 1-5$  at  $\omega_0 t = 25000$ .  $S(0) = |s_i|^2$  is fixed at 1.

In Fig. 3, we plot the scaled energy moments

$$U_n = \langle U^n \rangle \exp \left[ -n(n+1) \left( \frac{g\omega_0 t}{4} \right) \right], \quad (23)$$

for  $n = 1, 2, 3, 4$ . In the long-time regime ( $\omega_0 t \gtrsim g^{-1}$ ), these values converge accurately to  $n!/(2n-1)!!$  up to  $\omega_0 t \sim 10^6$ . Beyond this point, deviations emerge due to the rapid growth of  $\langle U^n \rangle$  and the accumulation of numerical errors.

To characterize the reflectance distribution more precisely, we evaluate the dimensionless quantity

$$F_3 = \frac{\langle R^3 \rangle \langle R \rangle^3}{\langle R^2 \rangle^3}, \quad (24)$$

which eliminates time-dependent scaling and isolates the distribution's intrinsic form. The value of  $F_3$  serves as a

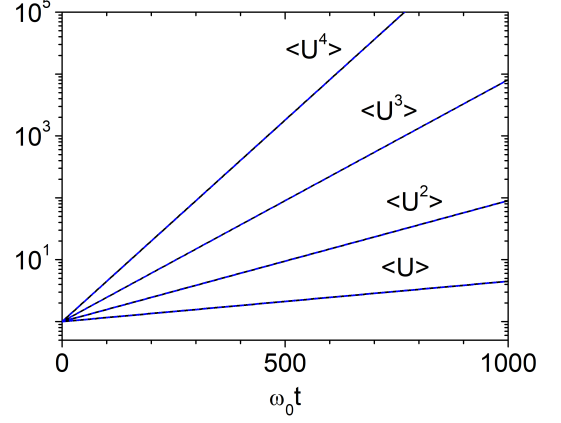


FIG. 6. Temporal growth of energy moments for  $g = 0.003$  with  $R(0) = S(0) = 1/2$ . Solid lines show numerical results from Eq. (10); dashed lines indicate the analytical prediction from Eq. (22). The results confirm that the energy follows a log-normal distribution at all times when the initial waves propagate in opposite directions with equal amplitudes.

diagnostic:  $F_3 = 5/9 \approx 0.556$  for a gamma distribution,  $0.75$  for an exponential,  $1$  for a log-normal, and  $1.35$  for the quasi-log-normal form given by Eq. (20). As shown in Fig. 4, three distinct temporal regimes emerge: gamma-like for  $\omega_0 t \lesssim 1$ , exponential for  $1 \lesssim \omega_0 t \lesssim g^{-1}$ , and quasi-log-normal for  $g^{-1} \lesssim \omega_0 t \lesssim 10^6$ . Notably,  $F_3$  never reaches  $1$ , indicating that  $R$  does not follow a true log-normal distribution. A similar trend is observed in the wave energy, with  $\langle U^3 \rangle \langle U \rangle^3 / \langle U^2 \rangle^3 \approx 1.35$  at long times, consistent with quasi-log-normal statistics. Since  $g = g_0 \omega_0$ , the crossover from exponential to quasi-log-normal behavior occurs at a time scale proportional to  $g_0^{-1} \omega_0^{-2}$ .

The statistical behavior is highly sensitive to the initial conditions. When waves initially propagate in both directions, the moments are determined by the initial condition  $Z_{abcd}(0) = r_i^a (r_i^*)^b s_i^c (s_i^*)^d$ , with  $r_i$  and  $s_i$  defined in Eq. (13). The resulting statistics depend on the relative magnitudes of  $r_i$  and  $s_i$ . Figure 5 shows the scaled moments  $U_n$  ( $n = 1$  to  $5$ ) as functions of  $R(0) = |r_i|^2$  at  $\omega_0 t = 25000$ , with  $S(0) = |s_i|^2$  fixed at  $1$ . As  $R(0)$  increases from  $0$  to  $1$ —corresponding to symmetric bidirectional wave input—all  $U_n$  increase and converge to  $1$ . In this limit, the energy distribution becomes exactly log-normal, with  $U_n = 1$  for all  $n$ .

This behavior is confirmed in Fig. 6, which shows the first four moments of  $U$  for the symmetric case  $R(0) = S(0) = 1/2$ . The numerical results exhibit excellent agreement with the analytical prediction given by Eq. (22) at all times, confirming that the energy follows a log-normal distribution throughout the evolution.

We also carried out simulations using Model 2, where the random component  $\delta\epsilon$  remains constant over each time interval of duration  $\Lambda = 1/\omega_0$  and is abruptly updated at the end of each interval. Each value is independently sampled from a uniform distribution over

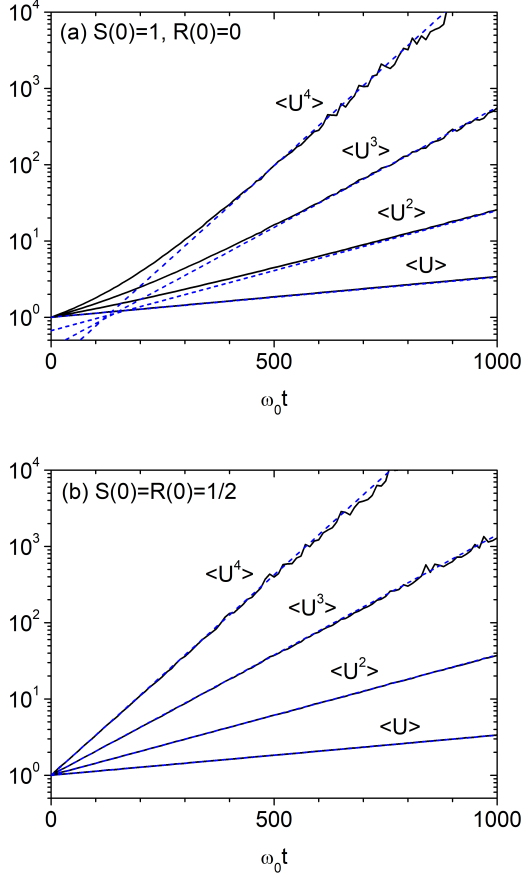


FIG. 7. Temporal growth of energy moments under stepwise disorder (Model 2) with  $\Lambda = 1/\omega_0$  and  $a_0 = 0.1$ . Effective disorder strengths of  $g \approx 0.00246$  (unidirectional input) and  $g \approx 0.00242$  (symmetric bidirectional input) are obtained by fitting the exponential growth of  $\langle U \rangle$ . (a) Numerical results (solid lines) for unidirectional input [ $S(0) = 1$ ,  $R(0) = 0$ ] agree well with the analytical prediction from Eq. (20) (dashed lines) at long times. (b) For symmetric bidirectional input [ $S(0) = R(0) = 1/2$ ], numerical results match the analytical expression from Eq. (22) at all times.

$[-a_0, a_0]$ , with  $a_0 = 0.1$ . Equation (3) was solved for  $10^6$  independent realizations, and the results were ensemble averaged over the total duration  $T$ .

We find that the average energy  $\langle U \rangle$  grows exponentially at all times, independent of the initial condition. Fitting this growth yields an effective disorder strength of  $g \approx 0.00246$  for unidirectional input and  $g \approx 0.00242$  for symmetric bidirectional input. Using these fitted values, we compare the numerical results from Model 2 with the analytical predictions of Eqs. (20) and (22). As shown in Fig. 7(a), the energy moments for unidirectional input closely follow Eq. (20) in the long-time regime. For symmetric bidirectional input, the moments agree with the log-normal form of Eq. (22) at all times [Fig. 7(b)]. These results confirm that the observed statistical behavior is robust and largely independent of the specific disorder

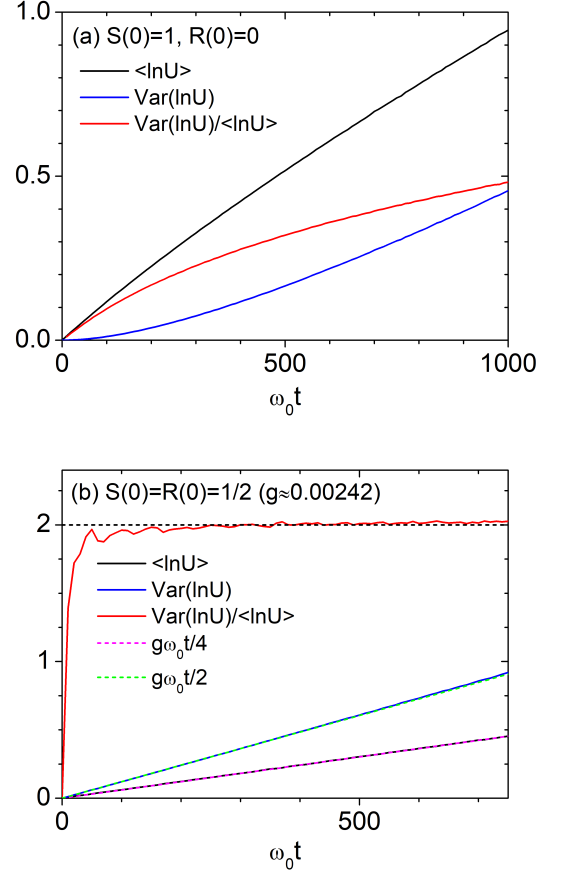


FIG. 8. Temporal evolution of  $\langle \ln U \rangle$ ,  $\text{Var}(\ln U)$ , and their ratio under stepwise disorder (Model 2) with  $\Lambda = 1/\omega_0$  and  $a_0 = 0.1$ . Results are averaged over  $10^6$  random configurations. (a) Unidirectional input [ $S(0) = 1$ ,  $R(0) = 0$ ]. (b) Symmetric bidirectional input [ $S(0) = R(0) = 1/2$ ] with effective disorder strength  $g \approx 0.00242$ , showing rapid convergence to the log-normal value  $\text{Var}(\ln U)/\langle \ln U \rangle = 2$ .

model used.

Using Model 2 with  $\Lambda = 1/\omega_0$  and  $a_0 = 0.1$ , we computed the mean and variance of  $\ln U$ . Figures 8(a) and 8(b) show  $\langle \ln U \rangle$ ,  $\text{Var}(\ln U)$ , and their ratio for unidirectional and symmetric bidirectional inputs. For symmetric input, the results align well with log-normal predictions:  $\langle \ln U \rangle = g\omega_0 t/4$ ,  $\text{Var}(\ln U) = g\omega_0 t/2$ , yielding a ratio of 2. In contrast, unidirectional input exhibits persistent deviations, with the ratio remaining well below 2 even at long times—indicating a clear departure from log-normal behavior.

Finally, we computed the probability distributions of  $\ln U$  and  $\ln R$  using Model 2 under stepwise disorder with  $\Lambda = 1/\omega_0$  and  $a_0 = 0.1$ , based on  $10^6$  independent simulations. Figures 9(a) and 9(b) present histogram-based probability density functions of  $\ln U$  and  $\ln R$  at various times for unidirectional input. Since  $U \geq 1$ ,  $\ln U$  is always positive, while  $\ln R$  can span the full real axis. The distribution of  $\ln U$  exhibits a clear crossover from

an exponential-like form to a quasi-log-normal shape. In contrast, the distribution of  $\ln R$  starts highly skewed and gradually becomes more symmetric over time. For symmetric bidirectional input [Fig. 9(c)], the distribution of  $\ln U$  remains Gaussian at all times, consistent with true log-normal behavior.

#### IV. DISCUSSION

Our study reveals that wave propagation in randomly time-varying media exhibits complex statistical behavior, distinct from that of spatially disordered systems. While previous work described temporal Anderson localization in terms of exponential and log-normal statistics [39], we show that this picture is incomplete. Crucially, the energy distribution is highly sensitive to the initial wave configuration—an aspect largely neglected in earlier analyses.

For unidirectional input, the statistics evolve through three regimes: a gamma distribution at early times, exponential behavior in the intermediate regime ( $1 \lesssim \omega_0 t \lesssim g^{-1}$ ), and a quasi-log-normal distribution at long times. The latter deviates from a true log-normal form due to a distinct prefactor in the moments, arising from temporal interference and amplitude fluctuations. In contrast, symmetric bidirectional input yields genuine log-normal statistics across all timescales, as confirmed by analytical results, numerical simulations, and agreement in scaled moments  $U_n$  and the ratio  $\text{Var}(\ln U)/\langle \ln U \rangle$ .

Momentum conservation constrains the dynamics: although the total energy grows due to temporal driving, the difference between reflected and transmitted energies remains fixed, linking the initial wave symmetry to long-term statistical behavior. Our findings are robust across two disorder models—delta-correlated Gaussian noise and stepwise uniform fluctuations—indicating that the observed statistics reflect universal features of temporally disordered systems rather than model-specific artifacts. These results have direct implications for dynamic wave control and device design. By engineering initial wave symmetry and temporal disorder, it is possible to tailor energy distributions for applications in photonic switching, robust energy confinement, and temporally programmable media.

Future research directions include extending this framework to spatiotemporal or nonlinear systems, where richer localization and interaction effects may arise. Experimental realization using metamaterials, time-modulated dielectrics, or plasmas could further validate and harness the statistical regimes identified in this work.

#### ACKNOWLEDGMENTS

This research was supported by the Basic Science Research Program through the National Research Foundation of Korea (<https://ror.org/013aysd81>) funded by the Ministry of Education (RS-2021-NR060141).

- 
- [1] D. L. Sounas and A. Alù, “Non-reciprocal photonics based on time modulation,” *Nat. Photonics*, vol. 11, p. 774, 2017.
  - [2] E. Galiffi *et al.*, “Photonics of time-varying media,” *Adv. Photonics*, vol. 4, p. 014002, 2022.
  - [3] M. H. Mostafa, M. S. Mirmoosa, M. S. Sidorenko, V. S. Asadchy, and S. A. Tretyakov, “Temporal interfaces in complex electromagnetic materials: An overview,” *Opt. Mater. Express*, vol. 14, p. 1103, 2024.
  - [4] M. M. Asgari *et al.*, “Theory and applications of photonic time crystals: A tutorial,” *Adv. Opt. Photonics*, vol. 16, p. 958, 2024.
  - [5] J. R. Zurita-Sánchez, P. Halevi, and J. C. Cervantes-González, “Reflection and transmission of a wave incident on a slab with a time-periodic dielectric function  $\epsilon(t)$ ,” *Phys. Rev. A*, vol. 79, p. 053821, 2009.
  - [6] E. Lustig, Y. Sharabi, and M. Segev, “Topological aspects of photonic time crystals,” *Optica*, vol. 5, p. 1390, 2018.
  - [7] T. T. Koutserimpas and R. Fleury, “Electromagnetic waves in a time periodic medium with step-varying refractive index,” *IEEE Trans. Antennas Propag.*, vol. 66, p. 5300, 2018.
  - [8] V. Pacheco-Peña and N. Engheta, “Temporal aiming,” *Light Sci. Appl.*, vol. 9, p. 129, 2020.
  - [9] V. Pacheco-Peña and N. Engheta, “Temporal equivalent of the Brewster angle,” *Phys. Rev. B*, vol. 104, p. 214308, 2021.
  - [10] V. Bacot, M. Labousse, A. Eddi, M. Fink, and E. Fort, “Time reversal and holography with spacetime transformations,” *Nat. Phys.*, vol. 12, p. 972, 2016.
  - [11] A. Akbarzadeh, N. Chamanara, and C. Caloz, “Inverse prism based on temporal discontinuity and spatial dispersion,” *Opt. Lett.*, vol. 43, p. 3297, 2018.
  - [12] V. Pacheco-Peña and N. Engheta, “Antireflection temporal coatings,” *Optica*, vol. 7, p. 323, 2020.
  - [13] F. R. Prudêncio and M. G. Silveirinha, “Synthetic axion response with space-time crystals,” *Phys. Rev. Appl.*, vol. 19, p. 024031, 2023.
  - [14] R. Tirole *et al.*, “Double-slit time diffraction at optical frequencies,” *Nat. Phys.*, vol. 19, p. 999, 2023.
  - [15] M. Lyubarov *et al.*, “Amplified emission and lasing in photonic time crystals,” *Science*, vol. 377, p. 425, 2022.
  - [16] D. M. Solis, R. Kastner, and N. Engheta, “Time-varying materials in the presence of dispersion: Plane-wave propagation in a Lorentzian medium with temporal discontinuity,” *Photonics Res.*, vol. 9, Art. no. 091842, 2021.
  - [17] S. A. R. Horsley, E. Galiffi, and Y.-T. Wang, “Eigenpulses of dispersive time-varying media,” *Phys. Rev. Lett.*, vol. 130, p. 203803, 2023.
  - [18] T. T. Koutserimpas and F. Monticone, “Time-varying media, dispersion, and the principle of causality,” *Opt. Mater. Express*, vol. 14, p. 1222, 2024.
  - [19] C. Rizza *et al.*, “Harnessing the natural resonances of

- time-varying dispersive interfaces,” *Phys. Rev. Lett.*, vol. 133, p. 186902, 2024.
- [20] S. F. Koufidis, T. T. Koutserimpas, F. Monticone, and M. W. McCall, “Electromagnetic wave propagation in time-periodic chiral media,” *Opt. Mater. Express*, vol. 14, p. 3006, 2024.
- [21] M. S. Mirmoosa, M. H. Mostafa, A. Norrman, and S. A. Tretyakov, “Time interfaces in bianisotropic media,” *Phys. Rev. Res.*, vol. 6, p. 1842, 2024.
- [22] Y. Pan, M.-I. Cohen, and M. Segev, “Superluminal  $k$ -gap solitons in nonlinear photonic time crystals,” *Phys. Rev. Lett.*, vol. 130, p. 233801, 2023.
- [23] R. Tirole *et al.*, “Second harmonic generation at a time-varying interface,” *Nat. Commun.*, vol. 15, p. 7752, 2024.
- [24] N. Konforty *et al.*, “Second harmonic generation and nonlinear frequency conversion in photonic time-crystals,” *Light Sci. Appl.*, vol. 14, p. 152, 2025.
- [25] E. Galiffi, P. A. Huidobro, and J. B. Pendry, “Broadband nonreciprocal amplification in luminal metamaterials,” *Phys. Rev. Lett.*, vol. 123, p. 206101, 2019.
- [26] S. A. R. Horsley and J. B. Pendry, “Quantum electrodynamics of time-varying gratings,” *Proc. Natl. Acad. Sci. U.S.A.*, vol. 120, p. e2302652120, 2023.
- [27] J. B. Pendry and S. A. R. Horsley, “QED in space-time varying materials,” *APL Quantum*, vol. 1, p. 020901, 2024.
- [28] P. Reck, C. Gorini, A. Goussev, V. Krueckl, M. Fink, and K. Richter, “Dirac quantum time mirror,” *Phys. Rev. B*, vol. 95, p. 165421, 2017.
- [29] V. Junk, P. Reck, C. Gorini, and K. Richter, “Floquet oscillations in periodically driven Dirac systems,” *Phys. Rev. B*, vol. 101, p. 134302, 2020.
- [30] F. Ok, A. Bahrami, and C. Caloz, “Electron scattering at a potential temporal step discontinuity,” *Sci. Rep.*, vol. 14, p. 5559, 2024.
- [31] Y. Zhou *et al.*, “Broadband frequency translation through time refraction in an epsilon-near-zero material,” *Nat. Commun.*, vol. 11, p. 2180, 2020.
- [32] F. Miyamaru *et al.*, “Ultrafast frequency-shift dynamics at temporal boundary induced by structural-dispersion switching of waveguides,” *Phys. Rev. Lett.*, vol. 127, p. 053902, 2021.
- [33] H. Moussa *et al.*, “Observation of temporal reflection and broadband frequency translation at photonic time interfaces,” *Nat. Phys.*, vol. 19, p. 863, 2023.
- [34] E. Lustig *et al.*, “Time-refraction optics with single cycle modulation,” *Nanophotonics*, vol. 12, p. 2221, 2023.
- [35] Z. Dong *et al.*, “Quantum time reflection and refraction of ultracold atoms,” *Nat. Photonics*, vol. 18, p. 68, 2024.
- [36] T. R. Jones, A. V. Kildishev, M. Segev, and D. Peroulis, “Time-reflection of microwaves by a fast optically-controlled time-boundary,” *Nat. Commun.*, vol. 15, p. 6786, 2024.
- [37] Y. Ren *et al.*, “Observation of momentum-gap topology of light at temporal interfaces in a time-synthetic lattice,” *Nat. Commun.*, vol. 16, p. 707, 2025.
- [38] Y. Sharabi, E. Lustig, and M. Segev, “Disordered photonic time crystals,” *Phys. Rev. Lett.*, vol. 126, p. 163902, 2021.
- [39] R. Carminati, H. Chen, R. Pierrat, and B. Shapiro, “Universal statistics of waves in a random time-varying medium,” *Phys. Rev. Lett.*, vol. 127, p. 094101, 2021.
- [40] B. Apffel, S. Wildeman, A. Eddi, and E. Fort, “Experimental implementation of wave propagation in disordered time-varying media,” *Phys. Rev. Lett.*, vol. 128, p. 094503, 2022.
- [41] J. Garnier, “Wave propagation in periodic and random time-dependent media,” *Multiscale Model. Simul.*, vol. 19, p. 1190, 2021.
- [42] J. Kim, D. Lee, S. Yu, and N. Park, “Unidirectional scattering with spatial homogeneity using correlated photonic time disorder,” *Nat. Phys.*, vol. 19, p. 726, 2023.
- [43] S. Kim and K. Kim, “Propagation of Dirac waves through various temporal interfaces, slabs, and crystals,” *Phys. Rev. Res.*, vol. 5, p. 023162, 2023.
- [44] K. S. Eswaran, A. E. Kopaei, and K. Sacha, “Anderson localization in photonic time crystals,” *Phys. Rev. B*, vol. 111, p. L180201, 2025.
- [45] S. Kim and K. Kim, “Spatial localization and diffusion of Dirac particles and waves induced by random temporal medium variations,” *Commun. Phys.*, vol. 8, p. 32, 2025.
- [46] S. Kim and K. Kim, “Invariant imbedding theory of wave propagation in arbitrarily inhomogeneous stratified bi-isotropic media,” *J. Opt.*, vol. 18, p. 065605, 2016.
- [47] S. Kim and K. Kim, “Giant overreflection of magneto-hydrodynamic waves from inhomogeneous plasmas with nonuniform shear flows,” *Phys. Fluids*, vol. 34, p. 127108, 2022.
- [48] K. Furutsu, “On the statistical theory of electromagnetic waves in a fluctuating medium (I),” *J. Res. Natl. Bur. Stand. D*, vol. 67, p. 303, 1963.
- [49] E. A. Novikov, “Functionals and the random-force method in turbulence theory,” *Sov. Phys. JETP*, vol. 20, p. 1290, 1965.



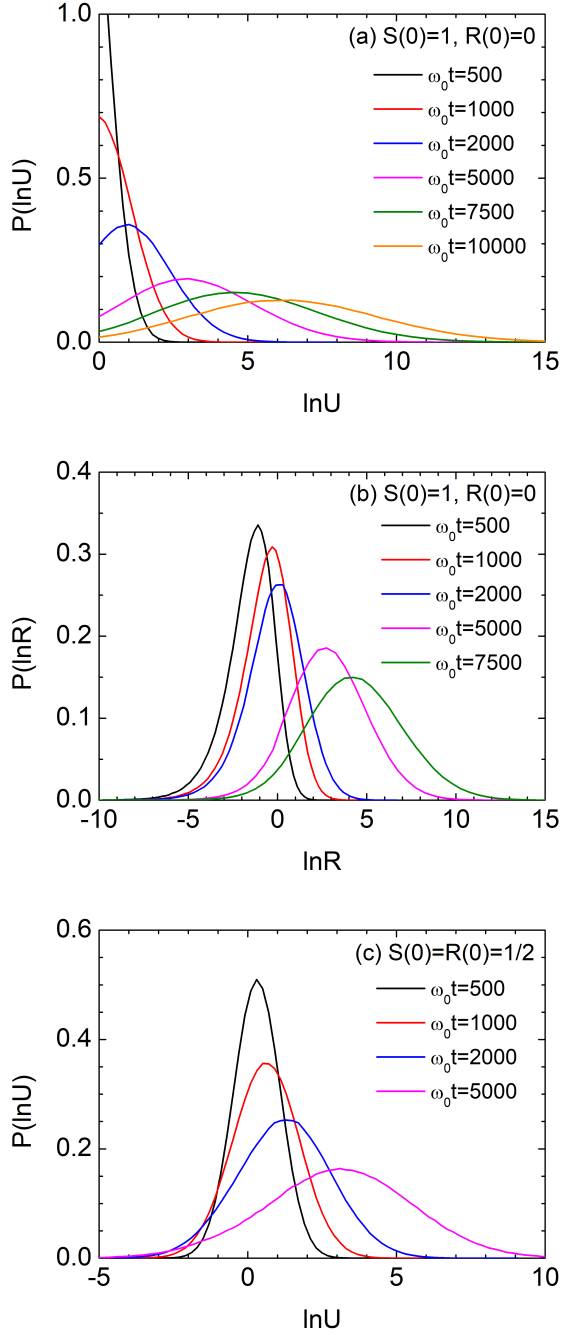


FIG. 9. Evolution of probability density functions under step-wise disorder (Model 2) with  $a_0 = 0.1$  and  $\Lambda = 1/\omega_0$ . (a,b) Distributions of  $\ln U$  and  $\ln R$  for unidirectional input, obtained from histograms of  $10^6$  samples at various times. (c) Distribution of  $\ln U$  for symmetric bidirectional input, showing Gaussian behavior consistent with log-normal statistics.